Nuclear Science and Techniques (2025) 36:239
https://doi.org/10.1007/s41365-025-01793-2

Effects of neutron excess in deformed Λ hypernuclei

Suo Qiu[1] · Huai-Tong Xue[2] · Xian-Rong Zhou[1]

Received: 5 February 2025 / Revised: 15 April 2025 / Accepted: 21 April 2025 / Published online: 9 October 2025

Abstract
The neutron excess effect, originating from the vanishing of one part of $\boldsymbol{\tau}_1 \cdot \boldsymbol{\tau}_2$ operator matrix elements, was appropriately considered within the Skyrme-type Λ*NN* three-body interactions and applied to the deformed SHF model. Analysis of a broad range of hypernuclei, from light to heavy masses, shows that the neutron excess effect significantly improves the description of Λ binding energies. The underlying mechanism involves reducing the Λ*NN* three-body repulsive interaction by subtracting the neutron excess term, thereby improving the binding energy of the hypernucleus. In addition, the impact of this effect on the Λ single-particle potential and the hyperon density distribution is discussed.

Keywords Λ hypernuclei · Skyrme-type Λ*N* interaction · Neutron excess · Isospin factor · Binding energy

1 Introduction

Since the identification of the first Λ hyperfragment in an emulsion exposed to cosmic rays in 1952 [1], Λ hypernuclei have been intensively studied, both experimentally [2–9] and theoretically [10–16]. Recent studies have mainly focused on hyperon–nucleon (*YN*) interactions [16–25], hypernuclear structure [15, 24, 26–31], hypernuclear decay [7, 32–38], and so on. Understanding the internal structure and *YN* interactions is a challenging goal in nuclear physics.

A single-Λ hypernucleus, which consists of a normal core nucleus and a Λ hyperon, provides a unique environment for investigating Λ*N* interactions. The degree of freedom of strangeness liberates the Λ hyperon from the constraints of the nuclear Pauli exclusion principle, allowing it to penetrate deeply into the nucleus and alter the core structure as an impurity. Therefore, the presence of impurity effects in the Λ hypernuclear system is crucial for illuminating nuclear features that might remain obscure in normal nuclei, including both the structure and interactions.

With the emergence of new and improved experimental facilities, the measurement of Λ hypernuclear binding energies spans a broad mass range from light to heavy with high resolution. These advancements not only enhance our understanding of Λ hypernuclear properties compared to previous studies but also pose challenges to the development and refinement of theoretical approaches in hypernuclear structures. To comprehensively describe these crucial nuclear properties, various types of Λ*N* interactions have been introduced and discussed. These include the Skyrme types [39–47], relativistic types [48–54], Nijmegen soft-core (NSC) types [55–57], Nijmegen extended-soft-core (ESC) types [13, 18, 21, 58–60], and chiral effective field theory (χEFT) types [22, 25, 61–63]. By using effective Λ–nucleon interactions, Λ hypernuclei have been comprehensively characterized within various nuclear models, including the antisymmetrized molecular dynamics model [30, 64–67], shell model [15, 68, 69], and mean field model [12, 31, 51–54, 70–78].

Over the past decades, two types of Λ*N* interactions have been proposed and adopted in the Skyrme–Hartree–Fock (SHF) model. The first type, derived from Brueckner–Hartree–Fock (BHF) calculations of hypernuclear matter, has

This work was supported by the National Natural Science Foundations of China (Nos. 12175071, 12575124, and 12505137), and Key Scientific Research Projects of Universities in Henan Province (No. 26B140011), and Doctoral Specialized Project of Nanyang Normal University (No. 2025ZX006).

✉ Huai-Tong Xue
htxue@nynu.edu.cn

✉ Xian-Rong Zhou
xrzhou@phy.ecnu.edu.cn

[1] Department of Physics, East China Normal University, Shanghai 200241, China

[2] College of Physics and Electronic Engineering, Nanyang Normal University, Nanyang 473061, China

a more microscopic basis. The second type is phenomenological Skyrme-type interactions, which are determined by fitting the experimental binding energies of Λ hypernuclei. Microscopic interactions originate from deeper physical principles (e.g., explicit momentum/density dependence). However, owing to the limited experimental data on Λ hypernuclei at present, microscopic interactions do not describe Λ hypernuclei very well. In contrast, phenomenological Skyrme-type interactions, which are determined by fitting the experimental binding energies of Λ hypernuclei, can better predict the ground-state properties of the hypernuclei.

Although Skyrme interactions provide a good description of hypernuclei, there are still some details that require improvement. For the Skyrme interaction, the parameter sets are RAY12 [39, 40], YBZ1 [42], SKSH2 [43], HPΛ2 [45], and SLL4 [47]. Different interactions were obtained by fitting different ground-state or excited-state energies of Λ hypernuclei. Moreover, different three-body interactions were considered in different Skyrme interactions. The Skyrme interaction with three-body interaction derived from the *G*-matrix can provide a good description of Λ hypernuclei ranging from light mass to heavy mass, such as SLL4 and HPΛ2. However, the Skyrme interaction with three-body interaction derived from the Λ*NN* contact force, like RAY12, YBZ1, and SKSH2, cannot provide a global description. A noticeable feature in the calculated results with the Λ*NN* contact force is that the parameters fitted to the binding energies of light-mass Λ hypernuclei, such as RAY12, YBZ1, and SKSH2, clearly fail to predict the experimental results for heavy-mass hypernuclei. Moreover, the calculated binding energies of heavy-mass Λ hypernuclei are smaller than the experimental values [77]. This underbinding shows that the Λ*N* potential depth is not sufficiently deep in heavy-mass Λ hypernuclei. This phenomenon is found not only in Skyrme interactions but also in other types of hyperon–nucleon interactions. For microscopic interactions, the calculated binding energies with the NSC89 interaction were smaller than the experimental results for heavy Λ hypernuclei [26]. The NSC97f interaction gives good results for heavy Λ hypernuclei, but its prediction for light Λ hypernuclei is approximately 2 MeV higher [26]. For the optical potential, the experimental binding energies of heavy Λ hypernuclei are larger than those calculated with the interaction obtained by fitting the 1*s* and 1*p* states of ${}^{16}_{\Lambda}$N [14]. Notably, the behavior of light-mass hypernuclei with symmetric nuclear matter core nuclei differs from that of heavy-mass hypernuclei with asymmetric nuclear matter core nuclei. This highlights the significant impact of isospin of the core nuclei on binding energy calculations.

In previous Skyrme-type interactions, only the simplest form of the contact Λ*NN* three-body interaction was considered [79]. However, an important feature of the Λ*NN* interaction is its proportionality to the isospin factor $\boldsymbol{\tau}_1 \cdot \boldsymbol{\tau}_2$ for the two nucleons involved [80]. Because of the isospin factor, Λ*NN* interaction between 'core' nucleons and 'excess' neutrons is suppressed when excess neutrons occupy shell-model orbits higher than those occupied by protons [14, 81]. By adding excess neutron, the influence of the isospin factor can be considered in the three-body interaction of Skyrme-type interactions. The three-body Λ*NN* interaction usually contributes significantly to the repulsion of *N*Λ forces, although there is no assurance that the three-body Λ*NN* interaction is universally repulsive. Therefore, the repulsive Λ*NN* interaction decreases owing to neutron excess, which is expected to solve the underbinding in heavy-mass Λ hypernuclei.

In the optical potential methodology [14, 81], the effects of neutron excess, considered using a more phenomenological approach, are discussed to address the underbinding issue in heavy-mass Λ hypernuclei. Deformation is a fundamental property of hypernuclei and has a significant impact on the B_Λ and other properties, especially for Λ states above the 1*s* state; therefore, it cannot be ignored. Furthermore, the pairing force is crucial in the calculation of nuclear properties [82]. In this study, the impact of neutron excess on deformed Λ hypernuclei is discussed in the framework of the SHF method with pairing force, which deals with the Bardeen–Cooper–Schrieffer (BCS) approximation.

The remainder of this paper is organized as follows: In Sect. 2, the theoretical method and interaction are briefly described. In Sect. 3, we discuss the binding energies of Λ hypernuclei and present the Λ single-particle potential along with the changes in the density distributions due to neutron excess. Finally, a summary is given in Sect. 4.

2 Theoretical descriptions

In the SHF approach, the total energy of a hypernucleus is given by [40, 83–87]

$$E = \int d^3\boldsymbol{r}\, \varepsilon(\boldsymbol{r}), \tag{1}$$

where the energy-density functional is

$$\varepsilon = \varepsilon_N[\rho_\mathrm{n}, \rho_\mathrm{p}, \tau_\mathrm{n}, \tau_\mathrm{p}, \boldsymbol{J}_\mathrm{n}, \boldsymbol{J}_\mathrm{p}] + \varepsilon_\Lambda[\rho_\mathrm{n}, \rho_\mathrm{p}, \rho_\Lambda, \tau_\Lambda, \boldsymbol{J}_N, \boldsymbol{J}_\Lambda], \tag{2}$$

with ε_N and ε_Λ as the contributions from *NN* and Λ*N* interactions, respectively. For the nucleonic functional ε_N, we used the standard Skyrme force SLy4 [88]. The one-body density ρ_q, kinetic density τ_q, and s.o. current $\boldsymbol{J}_q$ are

$$\left[\rho_q,\ \tau_q,\ \boldsymbol{J}_q\right] = \sum_{k=1}^{N_q} n_q^k \left[|\phi_q^k|^2,\ |\boldsymbol{\nabla}\phi_q^k|^2,\ \phi_q^{k*}(\boldsymbol{\nabla}\phi_q^k \times \boldsymbol{\sigma})/i\right], \tag{3}$$

where ϕ_q^k $(k = 1, \cdots, N_q)$ are the s.p. wave functions of the k-th occupied states for the different particles $q = \mathrm{n}, \mathrm{p}, \Lambda$. The occupation probabilities n_q^k were calculated by considering pairing within a BCS approximation for nucleons only. The pairing interaction between nucleons is considered as a density-dependent δ force [82, 89]:

$$V_q(\boldsymbol{r}_1, \boldsymbol{r}_2) = V_q' \left[1 - \frac{\rho_N((\boldsymbol{r}_1 + \boldsymbol{r}_2)/2)}{0.16\ \mathrm{fm}^{-3}}\right] \delta(\boldsymbol{r}_1 - \boldsymbol{r}_2)\,, \tag{4}$$

where pairing strengths $V_p' = V_n' = -410\ \mathrm{MeV\,fm}^3$ are used for light-mass nuclei [90], and $V_p' = -1146\ \mathrm{MeV\,fm}^3$, $V_n' = -999\ \mathrm{MeV\,fm}^3$ for medium-mass and heavy-mass nuclei [85]. A smooth energy cutoff was employed in the BCS calculations [91]. In the case of an odd number of nucleons, the orbit occupied by the unpaired nucleon is blocked, as described in Ref. [92].

Through the variation in the total energy, Eq. (1), one derives the SHF Schödinger equation for both nucleons and hyperons:

$$\left[-\boldsymbol{\nabla}\cdot\frac{1}{2m_q^*(\boldsymbol{r})}\boldsymbol{\nabla} + V_q(\boldsymbol{r}) - i\boldsymbol{W}_q(\boldsymbol{r})\cdot(\boldsymbol{\nabla}\times\boldsymbol{\sigma})\right]\phi_q^k(\boldsymbol{r}) = e_q^k\phi_q^k(\boldsymbol{r})\,, \tag{5}$$

where $V_q(\boldsymbol{r})$ is the central part of the mean field depending on the density and $\boldsymbol{W}_q(\boldsymbol{r})$ is the s.o. interaction part [83, 89].

For the Skyrme-type interactions, ε_Λ is given as [40, 42, 44, 46, 47]

$$\begin{aligned}\varepsilon_\Lambda =& \frac{\tau_\Lambda}{2m_\Lambda} + a_0\rho_\Lambda\rho_N + a_3\rho_\Lambda\rho_N^{1+\alpha} + a_3'\rho_\Lambda\left(\rho_N^2 + 2\rho_\mathrm{n}\rho_\mathrm{p}\right)\\ &+ a_1\left(\rho_\Lambda\tau_N + \rho_N\tau_\Lambda\right) - a_2\left(\rho_\Lambda\Delta\rho_N + \rho_N\Delta\rho_\Lambda\right)/2\\ &- a_4\left(\rho_\Lambda\boldsymbol{\nabla}\cdot\boldsymbol{J}_N + \rho_N\boldsymbol{\nabla}\cdot\boldsymbol{J}_\Lambda\right),\end{aligned} \tag{6}$$

where the last term is the s.o. part, which was adjusted to reproduce the observed s.o. splitting of ${}^{13}_{\Lambda}\mathrm{C}$ in our approach [31, 93, 94]. Previous studies [31] have shown that the effect of this term is small (0.1 MeV), which is ignored in this work. Two alternative parametrizations of nonlinear effects are indicated, that is, the first one a_3 motivated by a G-matrix [41, 45, 95] and the second one a_3' derived from a ΛNN contact force [39, 40]. In symmetric matter, the two choices are equivalent when $a_3 \equiv \frac{3}{2}a_3'$ and $\alpha = 1$ [46].

Then, one obtains the corresponding SHF mean fields:

$$\begin{aligned}V_\Lambda =& a_0\rho_N + a_1\tau_N - a_2\Delta\rho_N\\ &+ a_3\rho_N^{1+\alpha} + a_3'\left(\rho_N^2 + 2\rho_\mathrm{n}\rho_\mathrm{p}\right),\end{aligned} \tag{7}$$

$$\begin{aligned}V_\mathrm{n}^{(\Lambda)} =& a_0\rho_\Lambda + a_1\tau_\Lambda - a_2\Delta\rho_\Lambda\\ &+ a_3(1+\alpha)\rho_\Lambda\rho_N^\alpha + 2a_3'\rho_\Lambda(2\rho_N - \rho_\mathrm{n}),\end{aligned} \tag{8}$$

$$\begin{aligned}V_\mathrm{p}^{(\Lambda)} =& a_0\rho_\Lambda + a_1\tau_\Lambda - a_2\Delta\rho_\Lambda\\ &+ a_3(1+\alpha)\rho_\Lambda\rho_N^\alpha + 2a_3'\rho_\Lambda(2\rho_N - \rho_\mathrm{p}).\end{aligned} \tag{9}$$

In the previous Skyrme interactions [79], only the simplest form of the three-body interaction was considered, which is given by

$$t_{123} = \delta(\mathbf{r}_1 - \mathbf{r}_2)\delta(\mathbf{r}_3 - \mathbf{r}_1)t_3. \tag{10}$$

The three-body interaction is only related to the coordinates of the hyperons and nucleons. However, an important feature of the ΛNN interaction is its proportionality to the isospin factor $\boldsymbol{\tau}_1\cdot\boldsymbol{\tau}_2$ for the two nucleons involved [80]. Expanding the isospin operator in terms of raising and lowering operators within the matrix elements, we obtain

$$\begin{aligned}\sum_{ijk}\langle ijk|\boldsymbol{\tau}_i\cdot\boldsymbol{\tau}_j|ijk\rangle =& \sum_{\substack{i\in\text{ core}\\ j\in\text{ valence excess}}}\langle i|\tau_{iz}|i\rangle\langle j|\tau_{jz}|j\rangle\\ &+ \sum_{ij\in\text{others}}\langle ij|\tau_{iz}\tau_{jz}|ij\rangle\\ &+ \sum_{ij}\langle ij|\frac{\left(\tau_{i+}\tau_{j-} + \tau_{i-}\tau_{j+}\right)}{2}|ij\rangle,\end{aligned} \tag{11}$$

where i and j are the indices of the nucleons and k is the index of the Λ hyperon. 'core' refers to the isospin $T = 0$ part of nuclei, while 'valence excess' refers to the part of nuclei where excess neutrons occupy shell-model orbits higher than those occupied by protons. For each j, $\sum_{i\in\text{core}}\langle i|\tau_{iz}|i\rangle = 0$ since the isospin of the 'core' is zero. Therefore, the first term in Eqs. (11) vanishes: The third term in Eq. (11) is the exchange partner of such matrix elements that renormalize the two-body ΛN interaction [80]. Thus, the ΛNN interaction between 'core' nucleons and 'excess' neutrons is expected to be suppressed when the excess neutrons occupy shell-model orbits higher than those occupied by protons [14, 81]. By introducing excess neutrons, the effect of the isospin factor can be incorporated into the three-body interactions of the Skyrme-type interactions.

When excess neutrons occupy shell-model orbits that are higher than those occupied by protons, ρ_N is separated as:

$$\rho_N(r) = \rho^{\,\mathrm{c}}(r) + \rho^{\,\mathrm{v}}(r) = \rho_\mathrm{n}^{\,\mathrm{c}}(r) + \rho_\mathrm{p}^{\,\mathrm{c}}(r) + \rho_\mathrm{n}^{\,\mathrm{v}}(r), \tag{12}$$

where ρ^{c} refers to the Z protons plus the Z neutrons occupying the same nuclear 'core' orbits, and ρ^{v} refers to the $(N - Z)$ excess neutrons associated with the nuclear periphery [14, 81]. By deleting the cross term $\rho^{\mathrm{c}}\rho^{\mathrm{v}}$ to account for the neutron excess [14, 80, 81], Eqs.(6) and (7) can be rewritten as

$$\varepsilon_\Lambda = \frac{\tau_\Lambda}{2m_\Lambda} + a_0\rho_\Lambda\rho_N + a_3'\rho_\Lambda[2(\rho^c)^2 + 2(\rho^v)^2 - \rho_n^2 - \rho_p^2] + a_1\left(\rho_\Lambda\tau_N + \rho_N\tau_\Lambda\right) - \frac{a_2}{2}\left(\rho_\Lambda\Delta\rho_N + \rho_N\Delta\rho_\Lambda\right) - a_4\left(\rho_\Lambda\nabla\cdot J_N + \rho_N\nabla\cdot J_\Lambda\right), \tag{13}$$

$$V_\Lambda = a_0\rho_N + a_1\tau_N - a_2\Delta\rho_N + a_3'[2(\rho^c)^2 + 2(\rho^v)^2 - \rho_n^2 - \rho_p^2]. \tag{14}$$

We will keep Eqs. (8) and (9) are unchanged for the HF calculations because there is no cross term $\rho^c\rho^v$ in these equations.

In the present calculations, the deformed SHF Schrödinger equation was solved in cylindrical coordinates (r, z), under the assumption of axial symmetry of the mean fields. When compared with experimental deformations derived from the quadrupole moment Q_p, we employ the definition

$$\beta = \frac{\sqrt{5\pi}}{3}\frac{Q_p}{ZR_0^2} \tag{15}$$

with $R_0 \equiv 1.2A^{1/3}$ fm [87, 90, 96–98].

3 Results and discussion

In order to study the influence of neutron excess on Skyrme-type interaction RAY12, YBZ1, and SKSH2, we calculated the binding energies of Λ hypernuclei: ${}^{12}_{\Lambda}$B, ${}^{12}_{\Lambda}$C, ${}^{13}_{\Lambda}$C, ${}^{16}_{\Lambda}$N, ${}^{16}_{\Lambda}$O, ${}^{28}_{\Lambda}$Si, ${}^{32}_{\Lambda}$S, ${}^{51}_{\Lambda}$V, ${}^{89}_{\Lambda}$Y, ${}^{139}_{\Lambda}$La, and ${}^{208}_{\Lambda}$Pb.

Figure 1 shows the binding energies for the 1*s* and 1*p* states calculated with and without neutron excess compared to the experimental data. The red triangles show the results without neutron excess, blue squares show the results with neutron excess, and black circles show the experimental results from Ref. [99]. To better present the results of ${}^{12}_{\Lambda}$B, ${}^{12}_{\Lambda}$C, ${}^{16}_{\Lambda}$N and ${}^{16}_{\Lambda}$O, the results for ${}^{12}_{\Lambda}$C and ${}^{16}_{\Lambda}$O are displayed in the inset plots. It should be noted that not all hypernuclei in the figure contain excess neutrons. The results show that the highest neutrons occupy the shell-model orbit, which is lower than that of the highest protons in ${}^{12}_{\Lambda}$C, ${}^{16}_{\Lambda}$O, ${}^{28}_{\Lambda}$Si and ${}^{32}_{\Lambda}$S, while the highest neutrons occupy the same shell-model orbit as the highest protons in ${}^{13}_{\Lambda}$C. Therefore, the results for ${}^{12}_{\Lambda}$C, ${}^{13}_{\Lambda}$C, ${}^{16}_{\Lambda}$O, ${}^{28}_{\Lambda}$Si, and ${}^{32}_{\Lambda}$S remain unchanged regardless of the presence of neutron excess.

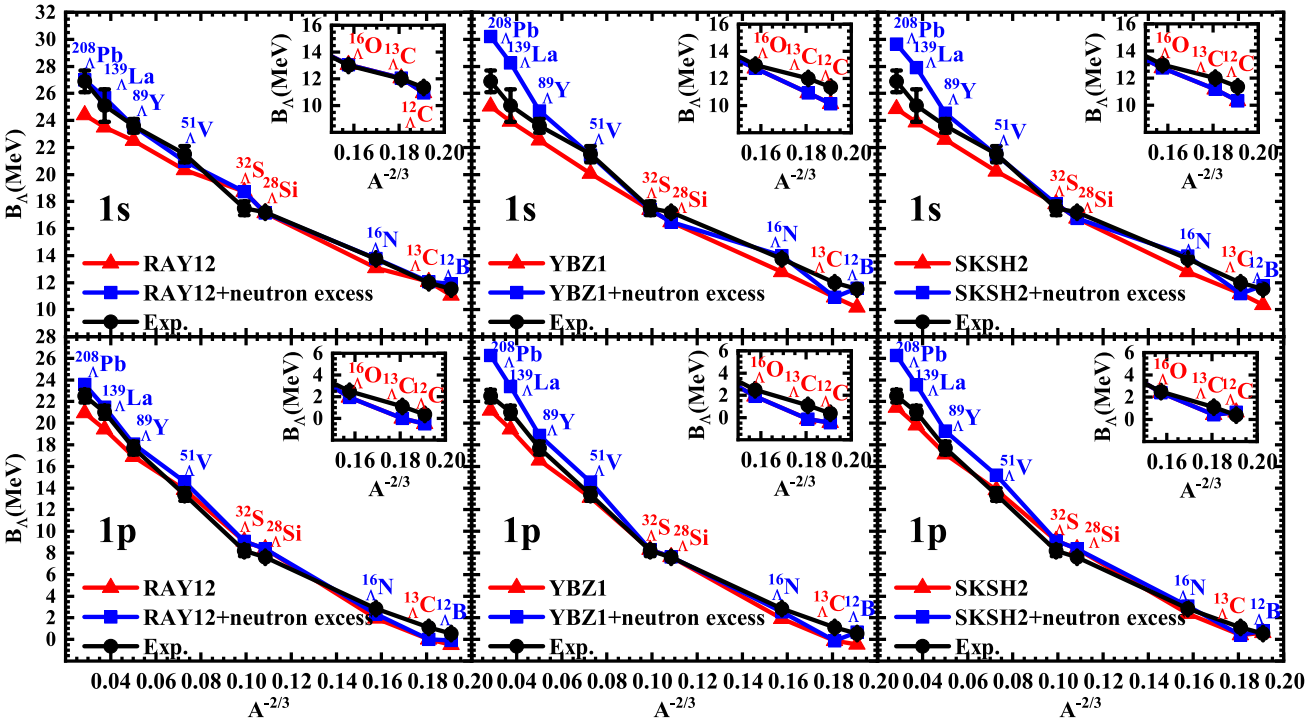

Fig. 1 (Color online) The binding energies (in MeV) of Λ 1*s* and 1*p* states of ${}^{12}_{\Lambda}$B, ${}^{12}_{\Lambda}$C, ${}^{13}_{\Lambda}$C, ${}^{16}_{\Lambda}$N, ${}^{16}_{\Lambda}$O, ${}^{28}_{\Lambda}$Si, ${}^{32}_{\Lambda}$S, ${}^{51}_{\Lambda}$V, ${}^{89}_{\Lambda}$Y, ${}^{139}_{\Lambda}$La, and ${}^{208}_{\Lambda}$Pb as calculated with and without neutron excess in Skyrme-type interaction RAY12, YBZ1 and SKSH2 compared with experimental data. The red triangles represent the results without neutron excess, the blue squares represent the results with neutron excess, and the black circles represent the experimental results including uncertainties from Ref. [99]. To enhance the visualization of the results for ${}^{12}_{\Lambda}$B, ${}^{12}_{\Lambda}$C, ${}^{16}_{\Lambda}$N, and ${}^{16}_{\Lambda}$O, the results for ${}^{12}_{\Lambda}$C and ${}^{16}_{\Lambda}$O are presented in inset plots.

It is clearly seen that the binding energies calculated using the Skyrme-type interactions RAY12, YBZ1, and SKSH2 failed to predict the experimental results in the heavy-mass hypernuclei. Moreover, the calculated binding energies in the heavy-mass Λ hypernuclei were smaller than the experimental values. This underbinding shows that the Λ*N* potential depth is not sufficiently deep in heavy-mass Λ hypernuclei. The reason for this phenomenon is that the parameter are fitted to the binding energies of the light-mass Λ hypernuclei. Therefore, the calculated results from the interaction exhibited poor agreement with the experimental values in the heavy-mass region. It is evident that the behavior of light-mass hypernuclei with symmetric nuclear matter core nuclei differs from that of heavy-mass hypernuclei with asymmetric nuclear matter core nuclei. Therefore, the influence of the isospin of the core nuclei on the binding energy calculations is significant. The Λ*NN* three-body is related to the isospin factor $\boldsymbol{\tau}_1 \cdot \boldsymbol{\tau}_2$ for the two nucleons involved [80]. The neutron excess reflects the influence of the isospin of core nuclei.

In Fig. 1, it is clear that the neutron excess slightly changes the binding energies of light-mass Λ hypernuclei with excess neutrons because excess neutrons are small in the light mass. Most importantly, neutron excess significantly increases the binding energies of heavy-mass Λ hypernuclei, because hypernuclei with heavy mass often have more excess neutrons. For the Skyrme-type interactions RAY12, YBZ1, and SKSH2, the interactions with neutron excess lead to better agreement with the experimental results of ${}^{12}_{\Lambda}$B and ${}^{16}_{\Lambda}$N. For the Skyrme-type interactions YBZ1 and SKSH2, although the interaction with neutron excess leads to increased binding energies, the calculated results do not agree with the experimental results for heavy hypernuclei. For the interaction YBZ1, a_3' was determined by assuming 500 MeV·fm^6 and calculating the binding energies of ${}^{13}_{\Lambda}$C, ${}^{16}_{\Lambda}$O, ${}^{28}_{\Lambda}$Si, ${}^{40}_{\Lambda}$Ca, ${}^{51}_{\Lambda}$V, and ${}^{89}_{\Lambda}$Y, which yielded good results, thereby confirming that a_3' was 500 MeV·fm^6 [42]. The interaction SKSH2 is fitted to binding energies of ${}^{12}_{\Lambda_{1s}}$C, ${}^{13}_{\Lambda_{1s}}$C, ${}^{13}_{\Lambda_{1p}}$C, ${}^{16}_{\Lambda_{1s}}$O, ${}^{16}_{\Lambda_{1p}}$O, ${}^{28}_{\Lambda_{1s}}$Si, ${}^{28}_{\Lambda_{1p}}$Si, ${}^{40}_{\Lambda_{1s}}$Ca, ${}^{40}_{\Lambda_{1p}}$Ca, ${}^{40}_{\Lambda_{1d}}$Ca, ${}^{51}_{\Lambda_{1s}}$V, ${}^{51}_{\Lambda_{1p}}$V, ${}^{51}_{\Lambda_{1d}}$V, ${}^{89}_{\Lambda_{1s}}$Y, ${}^{89}_{\Lambda_{1p}}$Y, ${}^{89}_{\Lambda_{1d}}$Y, ${}^{89}_{\Lambda_{1f}}$Y [43]. The two interactions, YBZ1 and SKSH2, were fitted to heavy-mass hypernuclei with asymmetric nuclear matter cores. The influence of asymmetric nuclear matter on the interaction parameters was relatively large. Therefore, these two interactions with neutron excess lead to the overbinding of hypernuclei. Compared to the interactions of YBZ1 and SKSH2, RAY12 is more suitable for studying this problem. The interaction of RAY12 was obtained without fitting heavy-mass hypernuclei with an asymmetric nuclear matter core. For Λ in 1*s* states, the calculated binding energies using RAY12 with neutron excess are in good agreement with the experimental data, especially for heavy hypernuclei, compared to those without neutron excess. For Λ in 1*p* states, it appears to work well, as shown by the significant improvement in the binding energies calculated using RAY12 with neutron excess for ${}^{12}_{\Lambda}$B, ${}^{16}_{\Lambda}$N, ${}^{89}_{\Lambda}$Y, ${}^{139}_{\Lambda}$La and ${}^{208}_{\Lambda}$Pb.

To check the overall description using RAY12 for all 11 hypernuclei, we calculate and list in Table 1 the average deviation $\bar{\chi}^2$ and the root mean square deviation Δ,

Table 1 The calculated binding energies (in MeV) of 1*s* and 1*p* states Λ for ${}^{12}_{\Lambda}$B, ${}^{12}_{\Lambda}$C, ${}^{13}_{\Lambda}$C, ${}^{16}_{\Lambda}$N, ${}^{16}_{\Lambda}$O, ${}^{28}_{\Lambda}$Si, ${}^{32}_{\Lambda}$S, ${}^{51}_{\Lambda}$V, ${}^{89}_{\Lambda}$Y, ${}^{139}_{\Lambda}$La and ${}^{208}_{\Lambda}$Pb with RAY12, RAY12+neutron excess and SLL4 in comparison with experimental values [99], along with the parameters of the Skyrme-type ΛN interactions. The values of $\bar{\chi}^2$ and Δ represent the average deviation and the root mean square deviation between the calculated binding energies of Λ hypernuclei and the experimental values. The root mean square deviation Δ is given in MeV

Hypernucleus	Exp	RAY12	RAY12+ neutron excess	SLL4
a_0		−237.40	−237.40	−322.00
a_1		–	–	15.75
a_2		−6.85	−6.85	19.63
a_3		–	–	715.00
a_3'		250.00	250.00	–
α		–	–	1.00
${}^{12}_{\Lambda_s}$B	11.52 ± 0.02	11.04	11.90	10.98
${}^{12}_{\Lambda_s}$C	11.36 ± 0.2	10.96	10.96	10.94
${}^{13}_{\Lambda_s}$C	12.0 ± 0.2	12.07	12.07	11.83
${}^{16}_{\Lambda_s}$N	13.76 ± 0.16	13.09	13.77	13.63
${}^{16}_{\Lambda_s}$O	13.0 ± 0.2	13.05	13.05	13.61
${}^{28}_{\Lambda_s}$Si	17.2 ± 0.2	17.16	17.16	17.68
${}^{32}_{\Lambda_s}$S	17.5 ± 0.5	18.72	18.72	18.74
${}^{51}_{\Lambda_s}$V	21.5 ± 0.6	20.33	20.99	21.39
${}^{89}_{\Lambda_s}$Y	23.6 ± 0.5	22.50	23.56	23.89
${}^{139}_{\Lambda_s}$La	25.1 ± 1.2	23.49	25.69	25.19
${}^{208}_{\Lambda_s}$Pb	26.9 ± 0.8	24.41	27.00	26.24
${}^{12}_{\Lambda_p}$B	0.54 ± 0.04	−0.48	−0.09	0.07
${}^{12}_{\Lambda_p}$C	0.36 ± 0.2	−0.51	−0.51	0.79
${}^{13}_{\Lambda_p}$C	1.1 ± 0.2	0.00	0.00	0.49
${}^{16}_{\Lambda_p}$N	2.84 ± 0.18	1.95	2.34	2.61
${}^{16}_{\Lambda_p}$O	2.5 ± 0.2	1.93	1.93	2.61
${}^{28}_{\Lambda_p}$Si	7.6 ± 0.2	8.36	8.36	8.73
${}^{32}_{\Lambda_p}$S	8.2 ± 0.5	9.08	9.08	9.48
${}^{51}_{\Lambda_p}$V	13.4 ± 0.6	13.85	14.59	14.44
${}^{89}_{\Lambda_p}$Y	17.7 ± 0.6	16.89	18.07	17.93
${}^{139}_{\Lambda_p}$La	21 ± 0.6	19.45	21.48	20.78
${}^{208}_{\Lambda_p}$Pb	22.5 ± 0.6	20.95	23.59	22.47
$\bar{\chi}^2$		63.09	31.86	42.83
Δ		1.06	0.66	0.61

$$\bar{\chi}^2 = \frac{1}{N}\sum_i^N \left(\frac{B^{\text{exp.}}_{\Lambda,i} - B^{\text{cal.}}_{\Lambda,i}}{\Delta B^{\text{exp.}}_{\Lambda,i}} \right)^2,$$
$$\Delta = \sqrt{\frac{1}{N}\sum_i^N \left(B^{\text{exp.}}_{\Lambda,i} - B^{\text{cal.}}_{\Lambda,i} \right)^2}, \tag{16}$$

with $N = 22$. From Table 1, it can be seen that the average deviation $\bar{\chi}^2$ and root mean square deviation Δ of the binding energies for Λ $1s$ and $1p$ states in the selected hypernuclei are shown for different Skyrme-type interactions. SLL4 is a recently developed ΛN Skyrme-type interaction that effectively describes hypernuclei across the entire periodic table using a single set of four parameters [46, 47]. By analyzing the $\bar{\chi}^2$ and Δ, it is evident that the inclusion of neutron excess improves the ability of RAY12 to describe the binding energies of hypernuclei. The key point to emphasize is that all the calculations were conducted without adjusting any parameters. Compared with SLL4, RAY12, which incorporates neutron excess, shows a smaller $\bar{\chi}^2$ and a similar Δ, while requiring fewer parameters. Therefore, with RAY12 plus neutron excess, the calculated binding energies of Λ $1s$ and $1p$ states are very close to the experimental values, indicating reasonably good agreement. This demonstrates the importance of neutron excess when excess neutrons occupy shell-model orbits that are higher than those occupied by protons.

Table 2 lists the quadrupole deformation parameters β and the binding energies of the Λ $1s$ and $1p$ states for various hypernuclei, comparing deformed results with their spherical counterparts (values in brackets). The data reveal that deformation has a significant impact on the binding energy, particularly for hypernuclei in the $1p_\Lambda$ state. For instance, for ${}^{16}_{\Lambda_p}$N and ${}^{16}_{\Lambda_p}$O, the binding energies differ noticeably between deformed and spherical calculations, with the deformed values being closer to experimental data. Conversely, the $1s_\Lambda$ state shows minimal differences, as the wave function of hyperon tends to be spherical in this state. These results show the necessity of considering deformation effects.

Figure 2 shows the Λ single-particle potential as a function of the radial distance r (fm) in the $z = 0$ plane for hypernuclei ${}^{51}_{\Lambda}$V, ${}^{89}_{\Lambda}$Y, ${}^{139}_{\Lambda}$La, and ${}^{208}_{\Lambda}$Pb. The red curves represent calculations without neutron excess (NE), whereas the blue curves represent neutron excess. Solid lines denote the total ΛN interactions, dashed lines indicate the two-body ΛN interactions, and dot-dashed lines indicate three-body ΛNN interactions. The neutron excess has almost no effect on the two-body ΛN interaction, but it effectively reduces the repulsive three-body ΛN interaction, thereby increasing the total ΛN interaction. Therefore, the hyperons are bound more deeply. The Λ-nuclear potential depth at zero momentum, $V_\Lambda(0)$, is -29.7 MeV, closely matching the -28 MeV depth derived from the simple Woods–Saxon (WS) attractive potential in Ref. [41].

Table 2 The calculated binding energies (in MeV) and the quadrupole deformation parameters β of Λ $1s$ and $1p$ states for ${}^{12}_{\Lambda}$B, ${}^{12}_{\Lambda}$C, ${}^{13}_{\Lambda}$C, ${}^{16}_{\Lambda}$N, ${}^{16}_{\Lambda}$O, ${}^{28}_{\Lambda}$Si, ${}^{32}_{\Lambda}$S, ${}^{51}_{\Lambda}$V, ${}^{89}_{\Lambda}$Y, ${}^{139}_{\Lambda}$La and ${}^{208}_{\Lambda}$Pb using RAY12 with neutron excess. The values in brackets are for spherical calculations

Hypernucleus	β	Binding energy
${}^{12}_{\Lambda_s}$B	−0.09	11.90 (11.95)
${}^{12}_{\Lambda_s}$C	−0.09	10.96 (10.97)
${}^{13}_{\Lambda_s}$C	0.00	12.07 (12.07)
${}^{16}_{\Lambda_s}$N	0.00	13.77 (13.77)
${}^{16}_{\Lambda_s}$O	0.00	13.05 (13.05)
${}^{28}_{\Lambda_s}$Si	−0.22	17.16 (17.21)
${}^{32}_{\Lambda_s}$S	0.00	18.72 (18.72)
${}^{51}_{\Lambda_s}$V	0.14	20.99 (20.95)
${}^{89}_{\Lambda_s}$Y	−0.02	23.56 (23.56)
${}^{139}_{\Lambda_s}$La	0.06	25.69 (25.90)
${}^{208}_{\Lambda_s}$Pb	0.00	27.00 (27.00)
${}^{12}_{\Lambda_p}$B	−0.21	−0.09 (−1.28)
${}^{12}_{\Lambda_p}$C	−0.207	−0.51 (−1.71)
${}^{13}_{\Lambda_p}$C	−0.15	0.00 (−0.42)
${}^{16}_{\Lambda_p}$N	0.07	2.34 (1.73)
${}^{16}_{\Lambda_p}$O	0.09	1.93 (1.06)
${}^{28}_{\Lambda_p}$Si	−0.26	8.36 (7.30)
${}^{32}_{\Lambda_p}$S	0.12	9.08 (8.62)
${}^{51}_{\Lambda_p}$V	0.17	14.59 (13.69)
${}^{89}_{\Lambda_p}$Y	−0.04	18.07 (17.95)
${}^{139}_{\Lambda_p}$La	0.06	21.48 (21.36)
${}^{208}_{\Lambda_p}$Pb	0.00	23.59 (23.59)

Figure 3 shows the rate of change in the hyperon density in the r-z plane due to neutron excess for four hypernuclei ${}^{51}_{\Lambda}$V, ${}^{89}_{\Lambda}$Y, ${}^{139}_{\Lambda}$La, and ${}^{208}_{\Lambda}$Pb. The rate of change in the hyperon density δ_Λ is given as

$$\delta_\Lambda \equiv \frac{\rho_\Lambda(\text{RAY12 + neutron excess}) - \rho_\Lambda(\text{RAY12})}{\rho_\Lambda(\text{RAY12})}. \tag{17}$$

The color scale represents the percentage change, with red and yellow indicating positive changes and green and blue showing negative changes. Neutron excess significantly affects the hyperon density distribution but has a minor impact on the core nucleus density distribution. Neutron excess leads to an increase in the central density of the hyperon and a decrease in the outer density, resulting in a decrease in the radius of the hyperon. Figure 4 illustrates the difference between neutron density and proton density, $\rho_n - \rho_p$, in the (r,z) plane for the hypernuclei ${}^{51}_{\Lambda}$V, ${}^{89}_{\Lambda}$Y, ${}^{139}_{\Lambda}$La, and ${}^{208}_{\Lambda}$Pb, respectively, calculated by the RAY12 interaction.

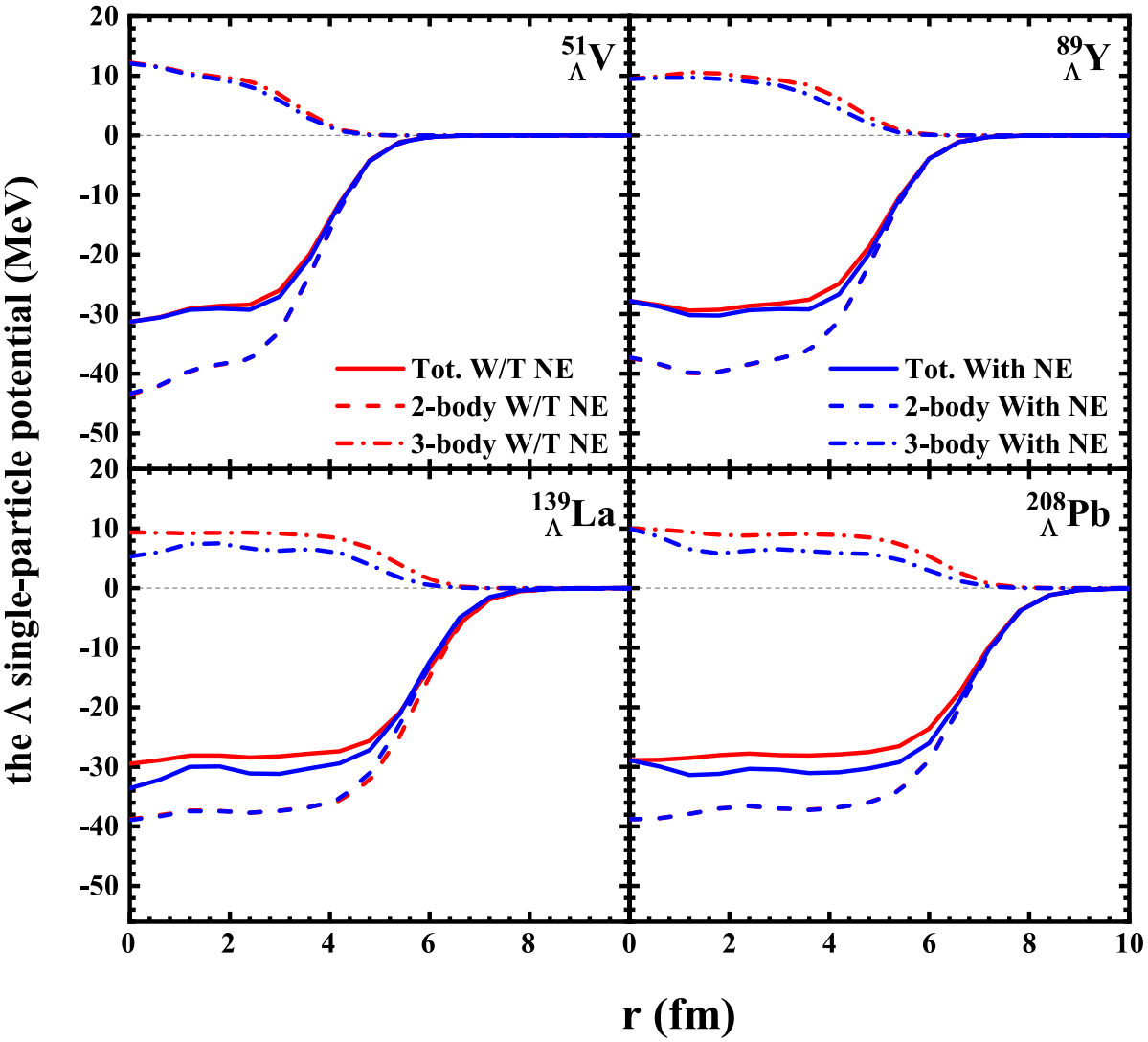

Fig. 2 (Color online) Two-body, three-body, and total Λ*N* interactions as functions of the radial distance r in the $z = 0$ plane in $^{51}_{\Lambda}$V, $^{89}_{\Lambda}$Y, $^{139}_{\Lambda}$La and $^{208}_{\Lambda}$Pb calculated using RAY12 with and without neutron excess. The red curves correspond to calculations without neutron excess (NE), while the blue curves account for neutron excess. Solid lines represent the total Λ*N* interactions, dashed lines illustrate the two-body Λ*N* interactions, and dot-dashed lines depict the three-body Λ*NN* interactions

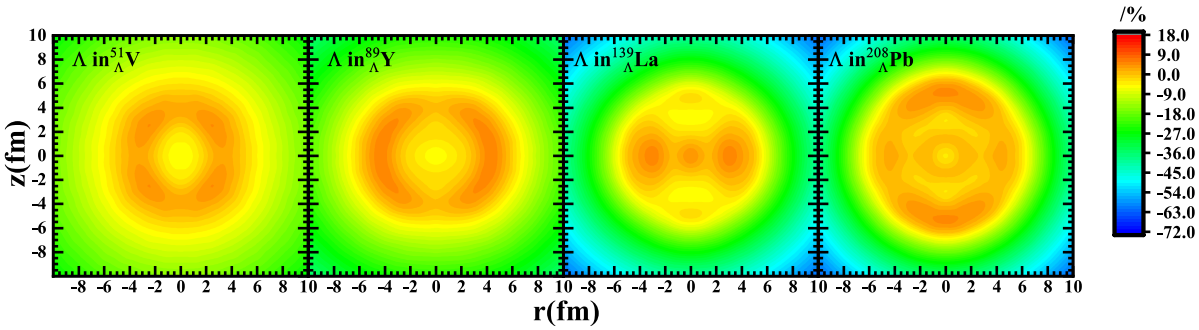

Fig. 3 (Color online) The changing rate of hyperon density δ_Λ, Eq. (17), in the (r, z) plane, for $^{51}_{\Lambda}$V, $^{89}_{\Lambda}$Y, $^{139}_{\Lambda}$La and $^{208}_{\Lambda}$Pb, obtained with the RAY12 interaction

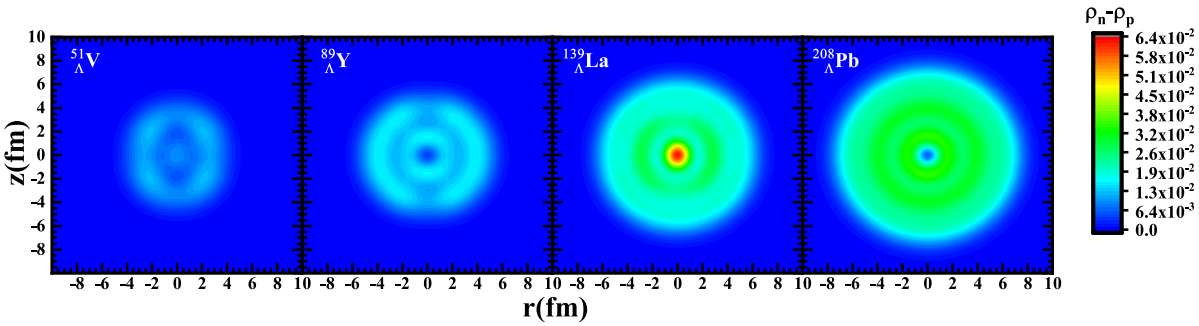

Fig. 4 (Color online) The difference between neutron density and proton density $\rho_n - \rho_p$, in the (r, z) plane, for $^{51}_{\Lambda}$V, $^{89}_{\Lambda}$Y, $^{139}_{\Lambda}$La and $^{208}_{\Lambda}$Pb, obtained with the RAY12 interaction

From Figs. 3 and 4, we find very similar shapes of δ_Λ and $\rho_n - \rho_p$ for $^{51}_{\Lambda}$V, $^{89}_{\Lambda}$Y, $^{139}_{\Lambda}$La, and $^{208}_{\Lambda}$Pb. This indicates that the effect of neutron excess is more significant in regions where the neutron density differs greatly from the proton density.

4 Summary

The effects of neutron excess on the Λ hypernuclei were studied by using the deformed SHF model in this work. Suppressing the Λ*NN* interaction between 'core' nucleons and 'excess' neutrons addresses underbinding in heavy-mass Λ hypernuclei. The microscopic mechanism can be explained as follows: the neutron excess decreases the repulsive Λ*NN* interaction, which can prevent this issue and be directly observed from the depth variation of the hyperon potential.

In addition, to quantitatively assess the impact of neutron excess, the binding energies of 1*s* and 1*p* Λ states for $^{12}_{\Lambda}$B, $^{12}_{\Lambda}$C, $^{13}_{\Lambda}$C, $^{16}_{\Lambda}$N, $^{16}_{\Lambda}$O, $^{28}_{\Lambda}$Si, $^{32}_{\Lambda}$S, $^{51}_{\Lambda}$V, $^{89}_{\Lambda}$Y, $^{139}_{\Lambda}$La and $^{208}_{\Lambda}$Pb were compared with those without the effect. Neutron excess significantly increases the B_Λ for heavy hypernuclei but has a less pronounced impact on light hypernuclei. In particular, for RAY12, good agreement was reached in this model between the calculated values and their corresponding experimental values considering the neutron excess effect.

By incorporating the isospin for the two nucleons into the three-body Λ*NN* interaction, a better prediction of the hypernuclear structure can be achieved. In the future, corrections for neutron excess will be introduced into the calculations of multi-Λ hypernuclei and Ξ hypernuclei (S=2).

Acknowledgements We would like to thank Prof. Sagawa for helpful discussions of the present work.

Author Contributions All authors contributed to the study conception and design. Material preparation, data collection, and analysis were performed by Suo Qiu, Huai-Tong Xue, and Xian-Rong Zhou. The first draft of the manuscript was written by Suo Qiu, who also contributed partially to methodology and conceptualization. Huai-Tong Xue participated partially in writing, review, editing, conceptualization, methodology, and funding acquisition. Xian-Rong Zhou was responsible for review and editing, supervision, project administration, and funding acquisition. All authors commented on previous versions of the manuscript.

Data Availability The data that support the findings of this study are openly available in Science Data Bank at https://cstr.cn/31253.11.sciencedb.j00186.00741 and https://doi.org/10.57760/sciencedb.j00186.00741.

Declarations

Conflict of interest The authors declare that they have no conflict of interest.

References

1. I. Lond, M. Danysz, J. Pniewski, Delayed disintegration of a heavy nuclear fragment. Edinburgh Dublin Philos. Magazine J. Sci. **44**, 348–350 (1953). https://doi.org/10.1080/14786440308520318
2. H. Tamura, S. Ajimura, H. Akikawa et al., γ-ray spectroscopy in Λ hypernuclei. Nucl. Phys. A **754**, 58–69 (2005). https://doi.org/10.1016/j.nuclphysa.2005.01.034
3. O. Hashimoto, H. Tamura, Spectroscopy of Λ hypernuclei. Prog. Part. Nucl. Phys. **57**, 564–653 (2006). https://doi.org/10.1016/j.ppnp.2005.07.001
4. A. Esser, S. Nagao, F. Schulz et al., Prospects for hypernuclear physics at Mainz: from KAOS@ MAMI to PANDA@ FAIR. Nucl. Phys. A **914**, 519–529 (2013). https://doi.org/10.1016/j.nuclphysa.2013.02.008
5. Y.G. Ma, Observation of antimatter nuclei at RHIC-STAR. J. Phys. Conf. Ser. **420**, 012036 (2013). https://doi.org/10.1088/1742-6596/420/1/012036
6. A. Feliciello, T. Nagae, Experimental review of hypernuclear physics: recent achievements and future perspectives. Rep. Prog. Phys. **78**, 096301 (2015). https://doi.org/10.1088/0034-4885/78/9/096301
7. M.S. Abdallah, B.E. Aboona, J. Adam et al., Measurements of H^3_Λ and H^4_Λ lifetimes and yields in Au+Au collisions in the high baryon density region. Phys. Rev. Lett. **128**, 202301 (2022). https://doi.org/10.1103/PhysRevLett.128.202301
8. B.E. Aboona, J. Adam, J.R. Adams et al., Observation of directed flow of hypernuclei H^3_Λ and H^4_Λ in $\sqrt{s_{NN}} = 3$ GeV Au+Au collisions at RHIC. Phys. Rev. Lett. **130**, 212301 (2023). https://doi.org/10.1103/PhysRevLett.130.212301

9. S.T.A.R. Collaboration, Observation of the antimatter hypernucleus ${}^{4}_{\bar{\Lambda}}\bar{\mathrm{H}}$. Nature **632**, 1026–1031 (2024). https://doi.org/10.1038/s41586-024-07823-0
10. B. Holzenkamp, K. Holinde, J. Speth, A meson exchange model for the hyperon-nucleon interaction. Nucl. Phys. A **500**, 485–528 (1989). https://doi.org/10.1016/0375-9474(89)90223-6
11. J. Schaffner, C.B. Dover, A. Gal et al., Multiply strange nuclear systems. Ann. Phys. **235**, 35–76 (1994). https://doi.org/10.1006/aphy.1994.1090
12. D.E. Lanskoy, Double-Λ hypernuclei in the Skyrme-Hartree-Fock approach and nuclear core polarization. Phys. Rev. C **58**, 3351 (1998). https://doi.org/10.1103/PhysRevC.58.3351
13. T.A. Rijken, M.M. Nagels, Y. Yamamoto, Status of understanding the YN/YY-interactions: Meson-exchange viewpoint. Nucl. Phys. A **835**, 160–167 (2010). https://doi.org/10.1016/j.nuclphysa.2010.01.189
14. E. Friedman, A. Gal, Constraints from Λ hypernuclei on the ΛNN content of the Λ-nucleus potential. Phys. Lett. B **837**, 137669 (2023). https://doi.org/10.1016/j.physletb.2023.137669
15. T. Myo, E. Hiyama, Structure of neutron-rich He Λ hypernuclei using the cluster orbital shell model. Phys. Rev. C **107**, 054302 (2023). https://doi.org/10.1103/PhysRevC.107.054302
16. H. Le, J. Haidenbauer, U.-G. Meißner et al., Light Λ hypernuclei studied with chiral hyperon-nucleon and hyperon-nucleon-nucleon forces. Phys. Rev. Lett. **134**, 072502 (2025). https://doi.org/10.1103/PhysRevLett.134.072502
17. E. Epelbaum, H.-W. Hammer, U.-G. Meißner, Modern theory of nuclear forces. Rev. Mod. Phys. **81**, 1773–1825 (2009). https://doi.org/10.1103/RevModPhys.81.1773
18. T.A. Rijken, M.M. Nagels, Y. Yamamoto, Baryon-baryon interactions—Nijmegen extended-soft-core models. Prog. Theor. Phys. Suppl. **185**, 14–71 (2010). https://doi.org/10.1143/PTPS.185.14
19. X.L. Ren, K.W. Li, L.S. Geng et al., Leading order relativistic chiral nucleon-nucleon interaction. Chin. Phys. C **42**, 014103 (2018). https://doi.org/10.1088/1674-1137/42/1/014103
20. K.W. Li, X.L. Ren, L.S. Geng et al., Leading order relativistic hyperon-nucleon interactions in chiral effective field theory. Chin. Phys. C **42**, 014105 (2018). https://doi.org/10.1088/1674-1137/42/1/014105
21. M.M. Nagels, T.A. Rijken, Y. Yamamoto, Extended-soft-core baryon-baryon model ESC16 III. S=–2 hyperon-hyperon/nucleon interactions. Phys. Rev. C **102**, 054003 (2020). https://doi.org/10.1103/PhysRevC.102.054003
22. J. Song, Z.-W. Liu, K.-W. Li et al., Test of the hyperon-nucleon interaction within leading order covariant chiral effective field theory. Phys. Rev. C **105**, 035203 (2022). https://doi.org/10.1103/PhysRevC.105.035203
23. Y.-G. Ma, Hypernuclei as a laboratory to test hyperon-nucleon interactions. Nucl. Sci. Tech. **34**, 97 (2023). https://doi.org/10.1007/s41365-023-01248-6
24. M. Knöll, R. Roth, Hyperon-nucleon interaction constrained by light hypernuclei. Phys. Lett. B **846**, 138258 (2023). https://doi.org/10.1016/j.physletb.2023.138258
25. J. Haidenbauer, U.-G. Meißner, A. Nogga et al., Hyperon-nucleon interaction in chiral effective field theory at next-to-next-to-leading order. Eur. Phys. J. A **59**, 63 (2023). https://doi.org/10.1140/epja/s10050-023-00960-6
26. I. Vidana, A. Polls, A. Ramos et al., Hypernuclear structure with the new Nijmegen potentials. Phys. Rev. C **64**, 044301 (2001). https://doi.org/10.1103/PhysRevC.64.044301
27. D.J. Millener, Hypernuclear structure from γ-ray spectroscopy. Nucl. Phys. A **754**, 48–57 (2005). https://doi.org/10.1016/j.nuclphysa.2004.12.068
28. E. Hiyama, T. Yamada, Structure of light hypernuclei. Prog. Part. Nucl. Phys. **63**, 339–395 (2009). https://doi.org/10.1016/j.ppnp.2009.05.001
29. J. Haidenbauer, I. Vidaña, Structure of single-Λ hypernuclei with chiral hyperon-nucleon potentials. Eur. Phys. J. A **56**, 55 (2020). https://doi.org/10.1140/epja/s10050-020-00055-6
30. M. Isaka, Y. Yamamoto, T. Motoba, Low-lying level structure of Λ hypernuclei and spin dependence of the Λ N interaction with antisymmetrized molecular dynamics. Phys. Rev. C **101**, 024301 (2020). https://doi.org/10.1103/PhysRevC.101.024301
31. H.T. Xue, Q.B. Chen, X.R. Zhou et al., Deformation and hyperon halo in hypernuclei. Phys. Rev. C **106**, 044306 (2022). https://doi.org/10.1103/PhysRevC.106.044306
32. E. Oset, L.L. Salcedo, Mesonic and non-mesonic Λ-decay in nuclei. Nucl. Phys. A **443**, 704–725 (1985). https://doi.org/10.1016/0375-9474(85)90220-9
33. K. Takeuchi, H. Takaki, H. Bandō, Nonmesonic decays of ${}^{4}_{\Lambda}$H, ${}^{4}_{\Lambda}$He and ${}^{5}_{\Lambda}$He hypernuclei by the π and ρ exchange model. Prog. Theor. Phys. **73**, 841–844 (1985). https://doi.org/10.1143/PTP.73.841
34. H. Noumi, S. Ajimura, H. Ejiri et al., Hypernuclear weak decay of ${}^{12}_{\Lambda}$C and ${}^{11}_{\Lambda}$B. Phys. Rev. C **52**, 2936 (1995). https://doi.org/10.1103/PhysRevC.52.2936
35. W.M. Alberico, G. Garbarino, Weak decay of Λ-hypernuclei. Phys. Rep. **369**, 1–109 (2002). https://doi.org/10.1016/S0370-1573(02)00199-0
36. Z.-Q. Feng, Formation and dynamics of exotic hypernuclei in heavy-ion collisions. Phys. Rev. C **102**, 044604 (2020). https://doi.org/10.1103/PhysRevC.102.044604
37. N. Buyukcizmeci, A.S. Botvina, R. Ogul et al., Evaluation of hypernuclei in relativistic ion collisions. Eur. Phys. J. A **56**, 1–15 (2020). https://doi.org/10.1140/epja/s10050-020-00217-6
38. Z.-Q. Feng, Extracting the hyperon-nucleon interaction via collective flows in heavy-ion collisions. Phys. Lett. B **851**, 138580 (2024). https://doi.org/10.1016/j.physletb.2024.138580
39. M. Rayet, Self-consistent calculations of hypernuclear properties with the Skyrme interaction. Ann. Phys. **102**, 226–251 (1976). https://doi.org/10.1016/0003-4916(76)90262-1
40. M. Rayet, Skyrme parametrization of an effective Λ-nucleon interaction. Nucl. Phys. A **367**, 381–397 (1981). https://doi.org/10.1016/0375-9474(81)90655-2
41. D.J. Millener, C.B. Dover, A. Gal, Λ-nucleus single-particle potentials. Phys. Rev. C **38**, 2700 (1988). https://doi.org/10.1103/PhysRevC.38.2700
42. Y. Yamamoto, H. Bandō, J. Žofka, On the Λ-hypernuclear single particle energies. Prog. Theor. Phys. **80**, 757–761 (1988). https://doi.org/10.1143/PTP.80.757
43. F. Fernandez, T. Lopez-Arias, C. Prieto, Skyrme-Hartree-Fock calculation of Λ-hypernuclear states from (π^+, K^+) reactions. Z. Phys. A **334**, 349–354 (1989). https://doi.org/10.1007/BF01284562
44. Y. Yamamoto, T. Motoba, T.A. Rijken, G-matrix approach to Hyperon-Nucleus systems. Prog. Theor. Phys. Suppl. **185**, 72–105 (2010). https://doi.org/10.1143/PTPS.185.72
45. N. Guleria, S.K. Dhiman, R. Shyam, A study of Λ hypernuclei within the Skyrme-Hartree-Fock model. Nucl. Phys. A **886**, 71–91 (2012). https://doi.org/10.1016/j.nuclphysa.2012.05.005
46. H.-J. Schulze, E. Hiyama, Skyrme force for light and heavy hypernuclei. Phys. Rev. C **90**, 047301 (2014). https://doi.org/10.1103/PhysRevC.90.047301
47. H.-J. Schulze, Skyrme forces for lambda and cascade hypernuclei. In AIP Conference Proceedings **2130**, 020009 (2019). https://doi.org/10.1063/1.5118377

48. Y. Sugahara, H. Toki, Relativistic mean field theory for lambda hypernuclei and neutron stars. Prog. Theor. Phys. **92**, 803–813 (1994). https://doi.org/10.1143/ptp/92.4.803
49. J. Mareš, B.K. Jennings, Relativistic description of Λ, Σ, and Ξ hypernuclei. Phys. Rev. C **49**, 2472 (1994). https://doi.org/10.1103/PhysRevC.49.2472
50. Z. Ma, J. Speth, S. Krewald et al., Hypernuclei with meson-exchange hyperon-nucleon interactions. Nucl. Phys. A **608**, 305–315 (1996). https://doi.org/10.1016/0375-9474(96)00169-8
51. Y. Tanimura, K. Hagino, Description of single-Λ hypernuclei with a relativistic point-coupling model. Phys. Rev. C **85**, 014306 (2012). https://doi.org/10.1103/PhysRevC.85.014306
52. R. Xu, C. Wu, Z. Ren, Single-Λ hypernuclei in the relativistic mean-field theory with parameter set FSU. J. Phys. G Nucl. Part. Phys. **39**, 085107 (2012). https://doi.org/10.1088/0954-3899/39/8/085107
53. X.S. Wang, H.Y. Sang, J.H. Wang et al., A new determination of the lambda-nucleon coupling constants in relativistic mean field theory. Commun. Theor. Phys. **60**, 479 (2013). https://doi.org/10.1088/0253-6102/60/4/16
54. Y.T. Rong, Z.H. Tu, S.G. Zhou, New effective interactions for hypernuclei in a density-dependent relativistic mean field model. Phys. Rev. C **104**, 054321 (2021). https://doi.org/10.1103/PhysRevC.104.054321
55. P.M.M. Maessen, T.A. Rijken, J.J. De Swart, Soft-core baryon-baryon one-boson-exchange models. II. Hyperon-nucleon potential. Phys. Rev. C **40**, 2226 (1989). https://doi.org/10.1103/PhysRevC.40.2226
56. T.A. Rijken, V.G.J. Stoks, Y. Yamamoto, Soft-core hyperon-nucleon potentials. Phys. Rev. C **59**, 21 (1999). https://doi.org/10.1103/PhysRevC.59.21
57. V.G.J. Stoks, T.A. Rijken, Soft-core baryon-baryon potentials for the complete baryon octet. Phys. Rev. C **59**, 3009 (1999). https://doi.org/10.1103/PhysRevC.59.3009
58. Y. Yamamoto, E. Hiyama, T.A. Rijken, Hypernuclear properties derived from the new interaction model ESC08. Nucl. Phys. A **835**, 350–353 (2010). https://doi.org/10.1016/j.nuclphysa.2010.01.216
59. T.A. Rijken, M.M. Nagels, Y. Yamamoto, Baryon-Baryon interactions S= 0,-1,-2,-3,-4: nijmegen extended-soft-core ESC08-models. Few-Body Syst. **54**, 801–806 (2013). https://doi.org/10.1007/s00601-013-0621-5
60. M.M. Nagels, T.A. Rijken, Y. Yamamoto, Extended-soft-core baryon-baryon model ESC16. II. Hyperon-nucleon interactions. Phys. Rev. C **99**, 044003 (2019). https://doi.org/10.1103/PhysRevC.99.044003
61. H. Polinder, J. Haidenbauer, U.-G. Meißner, Hyperon-nucleon interactions—a chiral effective field theory approach. Nucl. Phys. A **779**, 244–266 (2006). https://doi.org/10.1016/j.nuclphysa.2006.09.006
62. J. Haidenbauer, S. Petschauer, N. Kaiser et al., Hyperon-nucleon interaction at next-to-leading order in chiral effective field theory. Nucl. Phys. A **915**, 24–58 (2013). https://doi.org/10.1016/j.nuclphysa.2013.06.008
63. J. Haidenbauer, U.-G. Meißner, A. Nogga, Hyperon-nucleon interaction within chiral effective field theory revisited. Eur. Phys. J. A **56**, 91 (2020). https://doi.org/10.1140/epja/s10050-020-00100-4
64. M. Isaka, M. Kimura, A. Dote et al., Deformation of hypernuclei studied with antisymmetrized molecular dynamics. Phys. Rev. C **83**, 044323 (2011). https://doi.org/10.1103/PhysRevC.83.044323
65. M. Isaka, M. Kimura, Impurity effects of the Λ particle on the 2α cluster states of ^{9}Be and ^{10}Be. Phys. Rev. C **92**, 044326 (2015). https://doi.org/10.1103/PhysRevC.92.044326
66. M. Isaka, Y. Yamamoto, T.A. Rijken, Competing effects of nuclear deformation and density dependence of the ΛN interaction in B_Λ values of hypernuclei. Phys. Rev. C **94**, 044310 (2016). https://doi.org/10.1103/PhysRevC.94.044310
67. M. Isaka, Y. Yamamoto, T.A. Rijken, Effects of a hyperonic many-body force on B Λ values of hypernuclei. Phys. Rev. C **95**, 044308 (2017). https://doi.org/10.1103/PhysRevC.95.044308
68. H. Nemura, Y. Akaishi, Y. Suzuki, Ab initio approach to *s*-shell hypernuclei $^{3}_{\Lambda}$H, $^{4}_{\Lambda}$H, $^{4}_{\Lambda}$He and $^{5}_{\Lambda}$He with a ΛN-ΣN interaction. Phys. Rev. Lett. **89**, 142504 (2002). https://doi.org/10.1103/PhysRevLett.89.142504
69. H. Le, J. Haidenbauer, U.-G. Meißner et al., Jacobi no-core shell model for p-shell hypernuclei. Eur. Phys. J. A **56**, 1–20 (2020). https://doi.org/10.1140/epja/s10050-020-00314-6
70. Y. Tanimura, Clusterization and deformation of multi-Λ hypernuclei within a relativistic mean-field model. Phys. Rev. C **99**, 034324 (2019). https://doi.org/10.1103/PhysRevC.99.034324
71. W.Y. Li, J.W. Cui, X.R. Zhou, Structure of $^{9}_{\Lambda}$Be and $^{10}_{\Lambda\Lambda}$Be using the beyond-mean-field Skyrme-Hartree-Fock approach. Phys. Rev. C **97**, 034302 (2018). https://doi.org/10.1103/PhysRevC.97.034302
72. H. Mei, K. Hagino, J.M. Yao, Generator coordinate method for hypernuclear spectroscopy with a covariant density functional. Phys. Rev. C **93**, 011301 (2016). https://doi.org/10.1103/PhysRevC.93.011301
73. H. Mei, K. Hagino, J.M. Yao et al., Disappearance of nuclear deformation in hypernuclei: a perspective from a beyond-mean-field study. Phys. Rev. C **97**, 064318 (2018). https://doi.org/10.1103/PhysRevC.97.064318
74. H.T. Xue, Y.F. Chen, Q.B. Chen et al., Deformation and spin-orbit splitting of Λ hypernuclei in the Skyrme-Hartree-Fock approach. Phys. Rev. C **107**, 044317 (2023). https://doi.org/10.1103/PhysRevC.107.044317
75. H.T. Xue, Q.B. Chen, J.W. Cui et al., Structure of low-lying states of ^{12}C and $^{13}_{\Lambda}$C in a beyond-mean-field approach. Phys. Rev. C **109**, 024324 (2024). https://doi.org/10.1103/PhysRevC.109.024324
76. J. Guo, C.F. Chen, X.R. Zhou et al., ΛΛ pairing effects in spherical and deformed multi-Λ hyperisotopes. Phys. Rev. C **105**, 034322 (2022). https://doi.org/10.1103/PhysRevC.105.034322
77. C.F. Chen, Q.B. Chen, X.R. Zhou et al., Effects of Λ hyperons on the deformations of even-even nuclei. Chin. Phys. C **46**, 064109 (2022). https://doi.org/10.1088/1674-1137/ac5b58
78. Y.F. Chen, X.R. Zhou, Q.B. Chen et al., Lambda binding energies in the Skyrm Hartree-Fock approach with various Λ*N* interactions. Eur. Phys. J. A **58**, 21 (2022). https://doi.org/10.1140/epja/s10050-022-00672-3
79. T.H.R. Skyrme, The effective nuclear potential. Nucl. Phys. **9**, 615–634 (1958). https://doi.org/10.1016/0029-5582(58)90345-6
80. A. Gal, J.M. Soper, R.H. Dalitz, A shell-model analysis of Λ binding energies for the p-shell hypernuclei. I. Basic formulas and matrix elements for ΛN and ΛNN forces. Ann. Phys. **63**, 53–126 (1971)
81. E. Friedman, A. Gal, Λ hypernuclear potentials beyond linear density dependence. Nucl. Phys. A **1039**, 122725 (2023). https://doi.org/10.1016/j.nuclphysa.2023.122725
82. N. Tajima, P. Bonche, H. Flocard et al., Self-consistent calculation of charge radii of Pb isotopes. Nucl. Phys. A **551**, 434–450 (1993). https://doi.org/10.1016/0375-9474(93)90456-8
83. D. Vautherin, Hartree-Fock calculations with Skyrme's interaction. II. Axially deformed nuclei. Phys. Rev. C **7**, 296–316 (1973). https://doi.org/10.1103/PhysRevC.7.296
84. J. Cugnon, A. Lejeune, H.-J. Schulze, Hypernuclei in the Skyrme-Hartree-Fock formalism with a microscopic hyperon-nucleon force. Phys. Rev. C **62**, 064308 (2000). https://doi.org/10.1103/PhysRevC.62.064308

85. X.R. Zhou, H.-J. Schulze, H. Sagawa et al., Hypernuclei in the deformed Skyrme-Hartree-Fock approach. Phys. Rev. C **76**, 034312 (2007). https://doi.org/10.1103/PhysRevC.76.034312
86. X.R. Zhou, A. Polls, H.-J. Schulze et al., Λ hyperons and the neutron drip line. Phys. Rev. C **78**, 054306 (2008). https://doi.org/10.1103/PhysRevC.78.054306
87. H. Schulze, M.T. Win, K. Hagino et al., Hyperons as a probe of nuclear deformation. Prog. Theor. Phys. **123**, 569–580 (2010). https://doi.org/10.1143/PTP.123.569
88. E. Chabanat, P. Bonche, P. Haensel et al., A Skyrme parametrization from subnuclear to neutron star densities Part II. Nuclei far from stabilities. Nucl. Phys. A **635**, 231–256 (1998). https://doi.org/10.1016/S0375-9474(98)00180-8
89. M. Bender, K. Rutz, P.-G. Reinhard et al., Shell structure of superheavy nuclei in self-consistent mean-field models. Phys. Rev. C **60**, 034304 (1999). https://doi.org/10.1103/PhysRevC.60.034304
90. T. Suzuki, H. Sagawa, K. Hagino, Electromagnetic moments and electric dipole transitions in carbon isotopes. Phys. Rev. C **68**, 014317 (2003). https://doi.org/10.1103/PhysRevC.68.014317
91. M. Bender, K. Rutz, P.-G. Reinhard et al., Consequences of the center-of-mass correction in nuclear mean-field models. Eur. Phys. J. A **7**, 467–478 (2000). https://doi.org/10.1007/s100500050419
92. P. Ring, P. Schuck, *The nuclear many body problem* (Springer Verlag, Berlin, 1980)
93. M.Y. Win, K. Hagino, T. Koike, Shape of Λ hypernuclei in the (β, γ) deformation plane. Phys. Rev. C **83**, 014301 (2011). https://doi.org/10.1103/PhysRevC.83.014301
94. Y. Zhang, H. Sagawa, E. Hiyama, Hyperon halo structure of C and B isotopes. Phys. Rev. C **103**, 034321 (2021). https://doi.org/10.1103/PhysRevC.103.034321
95. D.E. Lanskoy, Y. Yamamoto, Skyrme-Hartree-Fock treatment of Λ and ΛΛ hypernuclei with *G*-matrix motivated interactions. Phys. Rev. C **55**, 2330–2339 (1997). https://doi.org/10.1103/PhysRevC.55.2330
96. S. Raman, C.W. Nestor, P. Tikkanen, Transition probability from the ground to the first-excited 2^+ state of even-even nuclides. Atom. Data Nucl. Data Tables **78**, 1–128 (2001). https://doi.org/10.1006/adnd.2001.0858
97. M.T. Win, K. Hagino, Deformation of Λ hypernuclei. Phys. Rev. C **78**, 054311 (2008). https://doi.org/10.1103/PhysRevC.78.054311
98. N.J. Stone, Table of nuclear electric quadrupole moments. Atom. Data Nucl. Data Tables **111**, 1–28 (2016). https://doi.org/10.1016/j.adt.2015.12.002
99. A. Gal, E.V. Hungerford, D.J. Millener, Strangeness in nuclear physics. Rev. Mod. Phys. **88**, 035004 (2016). https://doi.org/10.1103/RevModPhys.88.035004